

CAN THE STEEP MASS PROFILE OF A1689 BE EXPLAINED BY A TRIAXIAL DARK HALO?¹

MASAMUNE OGURI,^{2,3} MASAHIRO TAKADA,⁴ KEIICHI UMETSU,⁵ AND TOM BROADHURST⁶

Draft version December 2, 2024

ABSTRACT

The steep mass profile of A1689 derived from recent detailed lensing observations is not readily reconciled with the low concentration halos predicted by the standard cold dark matter (CDM) model. However, halo triaxiality may act to bias the profile constraints derived assuming a spherically symmetric mass distribution, since lensing relates only to the projected mass distribution. A degree of halo triaxiality is inherent to the CDM structure formation, arising from the collision-less nature of the dark matter. Here we compare the CDM-based model predictions of triaxial halo with the precise lensing measurements of A1689 based on the Advanced Camera for Surveys/Hubble Space Telescope and Subaru data, over a wide range of $10\text{kpc} \lesssim r \lesssim 2\text{Mpc}$. The model lensing profiles cover the intrinsic spread of halo mass and shape (concentration and triaxiality), and are projected over all inclinations when comparing with the data. We show that the model parameters are only weakly constrained and strongly degenerate mainly because of the lack of information along the line of sight. In particular, the limits on the concentration parameter become less restrictive with increasing triaxiality. Yet, by comparing the obtained constraints with expected probability distributions for the axis ratio and concentration parameters computed from numerical simulations, we find that $\sim 6\%$ of cluster-size halos in the CDM model can match the A1689 lensing observations at the $2\text{-}\sigma$ level, corresponding to cases where the major-axis of the halo is closely aligned with the line of sight. Thus halo triaxiality could reduce the apparent discrepancy between theory and observation. This hypothesis needs to be further explored by a statistical lensing study for other clusters as well as by complementary three-dimensional information derived using X-ray, kinematics, and Sunyaev-Zel'dovich effect observations.

Subject headings: cosmology – gravitational lensing – galaxies: clusters: individual (Abell 1689)

1. INTRODUCTION

The current standard model of structure formation, in which the universe is dominated by Cold Dark Matter (CDM), predicts that dark matter halos have an inner cusp that is shallower than a singular isothermal sphere model. Specifically, the radial density profile can be well fitted by an NFW profile $\rho(r) \propto r^{-1}(1+r/r_s)^{-2}$ (Navarro et al. 1997). An important parameter of this model is the concentration parameter c_{vir} , the ratio of the virial radius to the scale radius r_s . For massive clusters, it is predicted to be ~ 4 (e.g., Bullock et al. 2001). These are quite important predictions that should be confronted with observations.

Now it is becoming possible to *directly* test the NFW predictions using gravitational lensing. A poster child example for this is A1689: The inner mass distribution is tightly constrained from more than 100 multiple images of background galaxies discovered from the spectacular deep Advanced Camera for Surveys (ACS)/Hubble Space Telescope (HST) data (Broadhurst et al. 2005b, hereafter B05b), while the larger scale mass distribution up to the virial radius is obtained from the weak lensing measurements based on the wide-field Suprime-Cam/Subaru data (Broadhurst, Takada, Umetsu et al. 2005a, hereafter B05a). The two-dimensional mass profile of A1689, reconstructed from the combined lensing information, does continuously flatten towards the center like an NFW

profile, but the fitting to the NFW predictions leads to a surprisingly high concentration $c_{\text{vir}} = 14 \pm 1.5$ (B05a), compared with the expected value $c_{\text{vir}} \sim 4$. Such a high concentration is also seen in other clusters, e.g., MS2137-23 (Gavazzi et al. 2003) and possibly CL 0024+1654 (Kneib et al. 2003). These results may represent a new crisis in the current standard CDM model, offering a very rewarding issue to further explore.

However, the constraints above are obtained by deprojecting the two-dimensional lensing information under assumption of the spherically symmetric mass distribution. What the CDM model does predict is that dark halos are quite triaxial rather than spherical as a natural consequence of the collision-less dark matter nature and the filamentary nature of structure formation (Jing & Suto 2002, hereafter JS02; Lee et al. 2005). Therefore the results obtained assuming spherical symmetry might be biased (e.g., see Miralda-Escude & Babul 1995, for the similar discussion on A1689). In fact, Clowe et al. (2004) argued that the halo triaxiality affects both mass and concentration parameter measurements from gravitational lensing using N -body simulation results of clusters. Gavazzi (2005) also investigated the importance of the halo triaxiality and argued that a high concentration of MS2137-23 could be explained by a halo having the major axis oriented toward the line-of-sight.

In this paper, we study the mass distribution of A1689 based on triaxial dark halo model. Specifically, we adopt the triaxial halo model of JS02, and focus on whether the apparent steep mass profile of A1689 can be ascribed to triaxiality of the mass distribution. Throughout this paper we assume a concordance cosmology with the matter density $\Omega_M = 0.3$, the cosmological constant $\Omega_\Lambda = 0.7$, the dimensionless Hubble constant $h = 0.7$, and the normalization of matter power spectrum $\sigma_8 = 0.9$. Note that one arcminute corresponds to the

¹ Based in part on data collected at the Subaru Telescope, which is operated by the National Astronomical Society of Japan

² Princeton University Observatory, Peyton Hall, Princeton, NJ 08544

³ Department of Physics, University of Tokyo, Hongo 7-3-1, Bunkyo-ku, Tokyo 113-0033, Japan

⁴ Astronomical Institute, Tohoku University, Sendai 980-8578, Japan

⁵ Institute of Astronomy and Astrophysics, Academia Sinica, P. O. Box 23-141, Taipei 106, Taiwan, Republic of China

⁶ School of Physics and Astronomy, Tel Aviv University, Israel

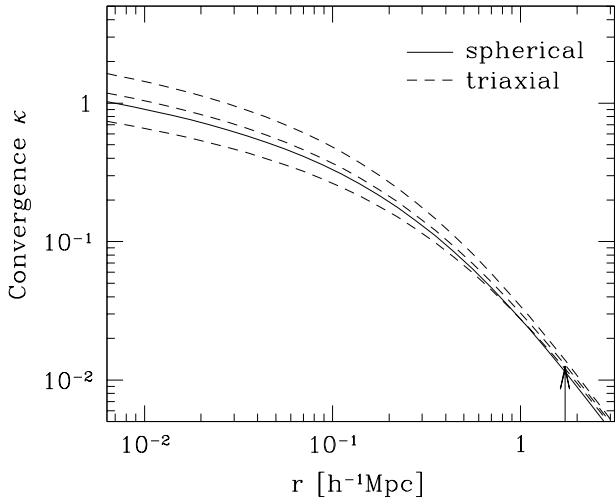


FIG. 1.— Convergence profiles of the triaxial halo with the virial mass $M_{\text{vir}} = 10^{15} h^{-1} M_{\odot}$, the concentration parameter $c_e = 1.15$, and the triaxial axis ratios of $a/c = 0.4$ and $b/c = 0.7$. The halo is placed at $z_l = 0.3$, and we assume the source redshift of $z_s = 1.0$. We consider the projection along each of the three principal axes: from upper to lower the dashed lines show profiles projected along z , y , and x (see eq. [1]). The convergence profile of the corresponding spherical NFW halo is also plotted by the solid line for comparison (see text for details). The vertical arrow indicates the virial radius.

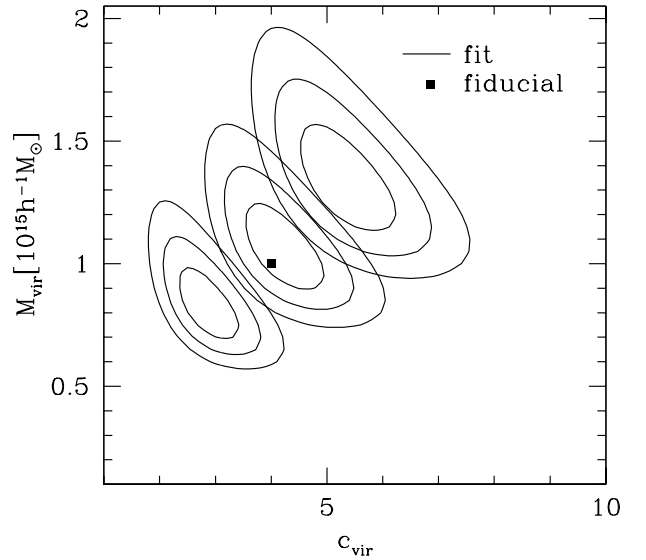


FIG. 2.— Constraint contours in the virial mass and halo concentration parameter space, obtained by fitting the mock data of triaxial halos to the spherical NFW halo model. The contours show 68%, 95%, 99.7% confidence limits (corresponding to $\Delta\chi^2 = 2.3, 6.17$ and 11.8 , respectively). From left to right, the constraint contours from the convergence profiles of the triaxial halo projected along the principal axes x , y , and z (as in Figure 1), respectively, are shown. For comparison, the square symbol shows the best-fitting model for the convergence profile obtained by projecting the *a priori* spherically-averaged mass profile of the input triaxial halo.

physical scale of $129 h^{-1} \text{kpc}$ for A1689 (redshift $z = 0.18$).

2. A SIMPLE ESTIMATION OF THE HALO TRIAXIALITY EFFECT ON LENSING MEASUREMENTS

Before going to the analysis of A1689, we make a simple test to demonstrate how important the halo triaxiality is in constraining mass profiles from a two-dimensional lensing measurement. The analysis is somewhat similar to that done by Clowe et al. (2004) who used high-resolution N -body simulations of massive clusters. Here we instead use an analytic model of aspherical dark halos.

We consider a triaxial halo with the virial mass $M_{\text{vir}} = 10^{15} h^{-1} M_{\odot}$ ⁷, placed at $z_l = 0.3$, and adopt the model mass profile given in JS02:

$$\rho(R) = \frac{\delta_{ce} \rho_{\text{crit}}(z)}{(R/R_0)(1+R/R_0)^2}, \quad (1)$$

$$R^2 \equiv c^2 \left(\frac{x^2}{a^2} + \frac{y^2}{b^2} + \frac{z^2}{c^2} \right) \quad (a \leq b \leq c). \quad (2)$$

We adopt typical model parameters for a halo of $10^{15} h^{-1} M_{\odot}$: the triaxial axis ratios are $a/c = 0.4$ and $b/c = 0.7$, and the concentration parameter $c_e \equiv R_e/R_0$, where R_e is defined such that the mean density enclosed within the ellipsoid of the major axis radius R_e is $\Delta_e \Omega(z) \rho_{\text{crit}}(z)$ with $\Delta_e = 5 \Delta_{\text{vir}} (c^2/ab)^{0.75}$, is chosen to be $c_e = 1.15$. We have checked that the spherically-averaged radial mass profile of the triaxial halo is quite similar to the spherical NFW profile that is specified by the virial radius $r_{\text{vir}} = R_e/0.45$, as proposed in JS02, and the concentration parameter $c_{\text{vir}} = 4$. However, it is non-trivial for these triaxial and spherical models whether to yield

similar lensing maps as a result of the line-of-sight projection⁸. To make this clear, Figure 1 compares the circularly-averaged convergence profiles for the spherical and triaxial halos. For the triaxial halo, we consider the projection along each of the three principal axes. It is clear that the surface mass density of the triaxial halo depends strongly on the projection direction. Therefore it is quite likely that adopting a spherical halo model causes a bias in estimating the mass and profile parameters for an individual cluster in reality.

To see this more clearly, we perform the following test. First, we generate an “observed” surface mass density profile: We consider 20 bins logarithmically spacing over the range $r = [10^{-2}, 1] h^{-1} \text{Mpc}$, and generate the convergence profile $\kappa(r)$, where the mean value for each bin is taken from the triaxial halo model and the Gaussian random error of standard deviation $\Delta(\log_{10} \kappa) = 0.1$ is added to each bin. Then, assuming the spherical NFW density profile, we constrain the virial mass (M_{vir}) and halo concentration parameter (c_{vir}) by fitting the model predictions to the “observed” profile. The constraint contours in the $M_{\text{vir}} - c_{\text{vir}}$ plane are shown in Figure 2, demonstrating that the best-fit parameters depend strongly on the projection direction. For example, the convergence profile projected along the major (minor) axis yields a significant overestimation (underestimation) by 20–30% in *both* the mass and concentration parameters. It should be noted that the bias direction is orthogonal to the degeneracy direction of the error ellipse, implying the systematics is very important. In fact, we fail to recover the model parameters of the spherically-averaged triaxial profile at more than $3\text{-}\sigma$ level when the halo is projected along the major- or minor-axis di-

⁷ The virial mass is defined by spherically averaging the halo mass distribution (the triaxial mass profile for our case) around the halo center and then by finding the sphere inside which the mean overdensity reaches Δ_{vir} predicted in the top-hat spherical collapse model.

⁸ The lensing convergence field $\kappa(\mathbf{r})$ is given in terms of the surface mass density $\Sigma(\mathbf{r})$ as $\kappa(\mathbf{r}) \equiv \Sigma(\mathbf{r})/\Sigma_{\text{cr}}$, where Σ_{cr} is the lensing critical density specified for a background cosmology and lens and source redshifts (see Schneider et al. 1992).

TABLE 1. BEST-FIT PARAMETERS FOR THE MODEL FITTING TO A1689

χ^2	R_e [Mpc]	c_e	a/c	b/c	$M_{\text{vir}}[10^{15}M_{\odot}]$
χ_{obs}^2	$1.80^{+0.08}_{-0.55}$	$7.6^{+1.0}_{-5.8}$	$0.1(< 0.75)$	$0.85(> 0.32)$	$1.8^{+0.4}_{-0.7}$
$\chi_{\text{obs}}^2 + \chi_{\text{fit}}^2$	$1.50^{+0.11}_{-0.12}$	$5.2^{+1.8}_{-1.9}$	$0.45^{+0.07}_{-0.10}$	$0.6^{+0.20}_{-0.15}$	$1.7^{+0.3}_{-0.2}$

NOTE. — Best-fit parameters and the 1- σ errors are presented, for the triaxial halo model fitting to the A1689 lensing information. Note that the virial mass M_{vir} is not a model parameter, but is derived from the constrained model parameters R_e , c_e , a/c , and b/c (see text for details). The lower row shows the results when the theoretically expected probability distributions for the axis ratios are employed as the priors of the fitting. For some parameters, only a lower or upper limit is obtained.

rections.

3. APPLICATION TO A1689

In this section, we indeed make a quantitative interpretation of the lensing measurements of A1689 in terms of the triaxial halo model in order to derive more reliable constraints on the three-dimensional mass distribution than does assuming the spherical halo model. Our particular attention is paid to whether or not the steep mass profile claimed in B05a can be reconciled with the CDM-based triaxial halo model of JS02.

Following the method of Oguri et al. (2003), the model lensing convergence field for a triaxial halo is specified by 7 parameters. As explained around equation (1), the virial radius of the triaxial halo modeling R_e , the concentration parameter c_e , and the axis ratio parameters a/c and b/c are considered. Further, we adopt three angle parameters to specify the halo orientation: θ , ϕ (see Figure 1 in Oguri et al. 2003) and the third angle between major axis of an ellipse of the projected mass distribution and the RA direction on the sky. Note that the parameter θ gives the angle between the major axis of the triaxial halo and the line-of-sight direction. We again note that, in this model, the virial mass M_{vir} is not a free parameter but is derivable from the model parameters (R_e , c_e , a/c , b/c). Throughout this paper, we assume $\langle z_s \rangle = 1$ for the mean redshift of source galaxies as done in B05a.

We then constrain the 7 model parameters from χ^2 fitting to the observed convergence map obtained from the ACS/HST and Suprime-Cam/Subaru data (e.g. see B05a for the similar method):

$$\chi_{\text{obs}}^2 = \chi_{\text{HST}}^2 + \chi_{\text{Subaru}}^2, \quad (3)$$

where we adopt flat priors of $0.1 \leq a/c (\leq 1)$ and $0.1 \leq b/c (\leq 1)$ for the axis ratios because a small axis ratio such as $a/c \leq 0.1$ is unrealistic for a virialized halo. For the ACS data, we use the circularly-averaged profile of the obtained convergence map that is given in 12 bins linearly spacing over the range $r = [0'.038, 0'.97]$ (see Figure 22 in B05b or Figure 3 in B05a)⁹. Hence, the χ_{HST}^2 is given by

$$\chi_{\text{HST}}^2 = \sum_{i=1}^{12} \frac{(\bar{\kappa}_i^{\text{m}} - \kappa_i)^2}{\sigma_i^2}, \quad (4)$$

where $\bar{\kappa}_i^{\text{m}}$ is the model prediction of the triaxial halo for the i -th radial bin, computed as in Figure 1, and the κ_i and σ_i are the observed value and 1- σ error, respectively. As for the Subaru data, we use the two-dimensional convergence map $\kappa(\mathbf{r})$ reconstructed from the joint measurements of the weak lensing distortion and magnification bias effects on background

⁹ It is not straightforward to use the two-dimensional mass map obtained from the ACS strong lensing analysis because of the complex, non-linear error propagation. The bin width of the one-dimensional convergence profile we use here is sufficiently broad to ensure that the errors between different bins are independent (B05b).

galaxies (Umetsu et al. 2005, in preparation). The map is given on $21 \times 17 (= 357)$ grids for the area of $\approx 30' \times 24'$. Note that the wide-field Subaru data allows us to probe the mass distribution on larger scales $\gtrsim 1'$ covering up to the virial radius $\sim 20'$ (B05a), thus ensuring that the ACS and Subaru information are independent. The pixel-pixel covariance matrix defined as $V_{ij} \equiv \langle \delta\kappa(\mathbf{r}_i) \delta\kappa(\mathbf{r}_j) \rangle$ can be accurately estimated based on the maximum likelihood map-making method, assuming that the error of weak lensing distortion arises from the random intrinsic ellipticities of background galaxies, while the magnification bias error is the Poissonian noise of the number counts (Schneider et al. 2000; see Umetsu et al. in preparation for the details). The χ_{Subaru}^2 can be therefore expressed as

$$\chi_{\text{Subaru}}^2 = \sum_{i,j} [\kappa^{\text{m}}(\mathbf{r}_i) - \kappa(\mathbf{r}_i)] (V^{-1})_{ij} [\kappa^{\text{m}}(\mathbf{r}_j) - \kappa(\mathbf{r}_j)], \quad (5)$$

where V^{-1} is the inverse of the covariance matrix.

Table 1 lists the best-fit values for the 4 model parameters of our interest as well as the virial mass derived, with the 1- σ error including the other 6 parameter uncertainties (estimated from $\Delta\chi^2 \equiv \chi^2 - \chi_{\text{min}}^2 = 1$ in the 7 parameter space). The minimum χ^2 is $\chi_{\text{min}}^2/\text{dof} = 378/362$ for 362 degrees of freedom, thus showing an acceptable fit. It is clear that the halo triaxiality significantly weakens constraints on the halo concentration parameter $c_e = 7.6^{+1.0}_{-5.8}$, compared to the constraint $c_{\text{vir}} = 14 \pm 1.5$ ($c_e \approx 0.45c_{\text{vir}}$) derived when *a priori* assuming the spherical NFW model (B05a). In fact, a smaller concentration compatible with the theoretical expectation $c_e = 1 - 2$ is marginally allowed at 1- σ level.

This is more clearly explored in Figure 3, which shows the error contours in the two parameter subspace. We also show the error contours in the $c_e - M_{\text{vir}}$ plane in Figure 4 to compare our result with Figure 3 of B05a. Apparently, the parameter constraints are significantly degenerate. For example, as a triaxial halo with smaller a/c is considered, a broader range of the halo concentration is allowed, implying that the lensing strength is as quite sensitive to the halo triaxiality as is to the halo concentration c_e . However, the axis ratios can be hardly constrained, obviously because of a lack of the halo shape information along the line-of-sight: Any values of a/c and b/c are allowed to within 3- σ level, though profiles close to spherical models ($a/c \sim 1$) are relatively disfavored because the Subaru convergence map is not circularly symmetric. More intriguing is that the degeneracy direction in the $c_e - M_{\text{vir}}$ plane (Figure 4) is almost orthogonal to that for the spherical case (Figure 3 in B05a), as illustrated in Figure 2. As a result, the mass constraint can be reconciled with the mass estimate derived from the X-ray observation ($\approx 1.0 \times 10^{15}M_{\odot}$ in Andersson & Madejski 2004) at 3- σ level. Thus the halo triaxiality could resolve the mass discrepancy reported in the literature (Miralda-Escude & Babul 1995; Andersson & Madejski

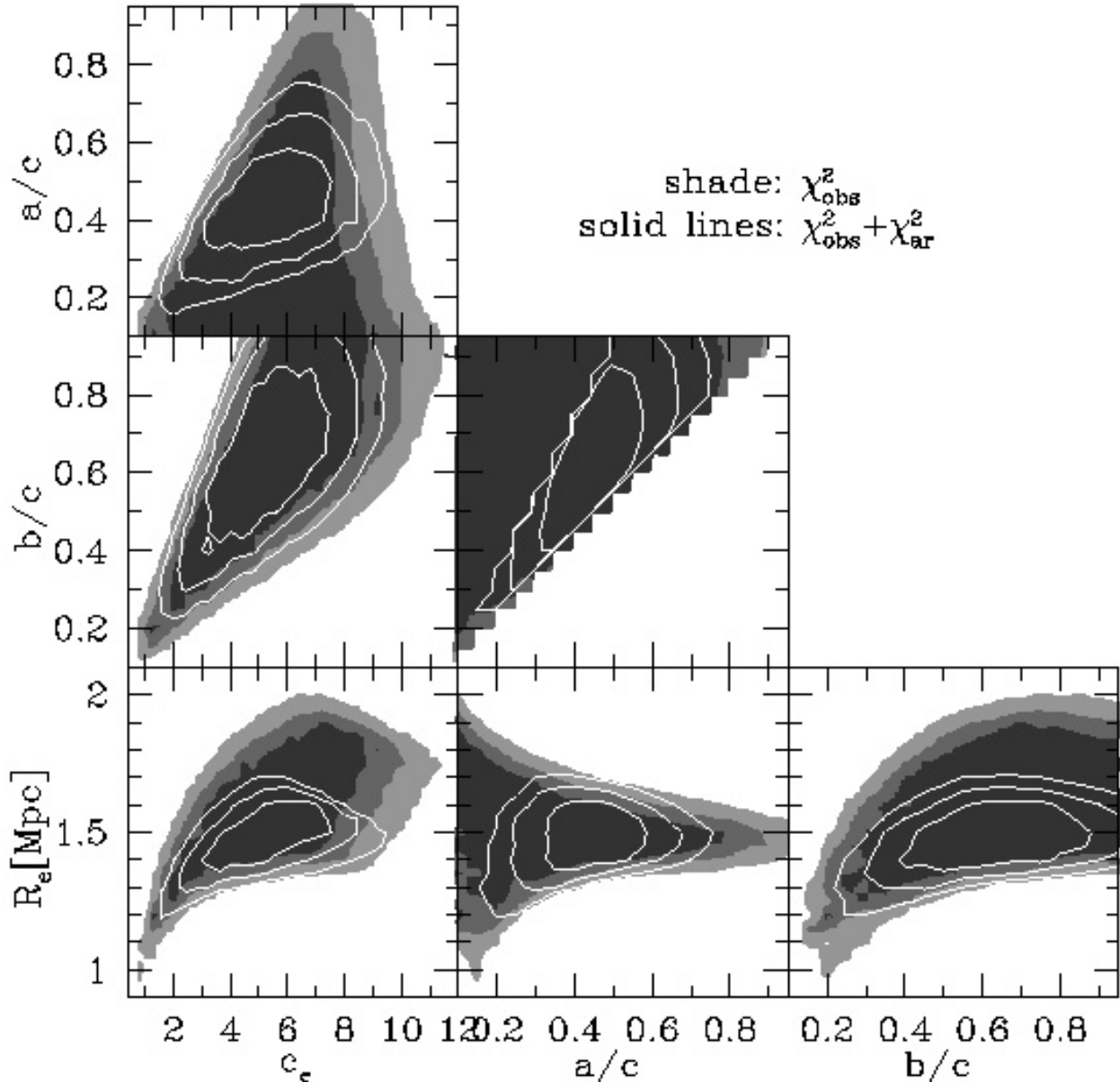


FIG. 3.— Projected constraint contours in the two parameter subspace from the 7 parameter space for the triaxial halo model, matching the two-dimensional mass distribution of A1689 reconstructed from the ACS/HST and Subaru data. The dark shaded regions show the 68%, 95% and 99.7% confidence intervals corresponding to $\Delta\chi^2 = 2.3, 6.17,$ and 11.8 in the 7 parameter space, respectively. It is clear that the parameter constraints are significantly weakened by inclusion of the halo triaxiality and show strong degeneracies in each parameter space. Note that the concentration parameter of the triaxial halo model, c_e , is approximately related to that of the spherical model via $c_e \simeq 0.45c_{\text{vir}}$ (JS02). The solid contours show the improved constraints when the CDM-based theoretical predictions of probability distributions for the axis ratios a/c and b/c are added as the prior to the χ^2 -fitting (see text for details). However, a broad range of the parameters are still allowed mainly because of a lack of the halo shape information along the line-of-sight.

2004; B05b), as we will again discuss later in more detail.

To improve the weak constraints above, we employ the prior knowledge of what kinds of halo shapes are expected for cluster-scale halos within the CDM clustering scenario. We use the probability distribution functions (PDFs) of the axis ratios, which are derived in JS02 using the N -body simulations. The PDFs are given as a function of redshift and halo mass; a cluster-scale halo at $z \approx 0$ is typically characterized by a triaxial shape with the mean value $a/c \approx 0.45$ and the standard deviation $\sigma(a/c) \approx 0.1$. For simplicity, we add the

following Gaussian prior to the χ^2 (eq. [3]):

$$\chi_{\text{ar}}^2 = -2.0 \ln [p(a/c)p(b/a|a/c)], \quad (6)$$

where the PDFs $p(a/c)$ and $p(b/a|a/c)$ are given by equations (17) and (19) in JS02, respectively. The resulting constraints are shown in Table 1 and Figures 3 and 4. However, the constraints are only weakly tightened and the main results we have so far found are not largely changed: a broad range of the halo concentration or the virial mass is still allowed.

Hence, to more highlight the constraint on the halo concentration, Figure 5 shows the error contours in the $c_e - a/c$ plane, when the radius R_e is fixed to $R_e = 1.4\text{Mpc}$ which is

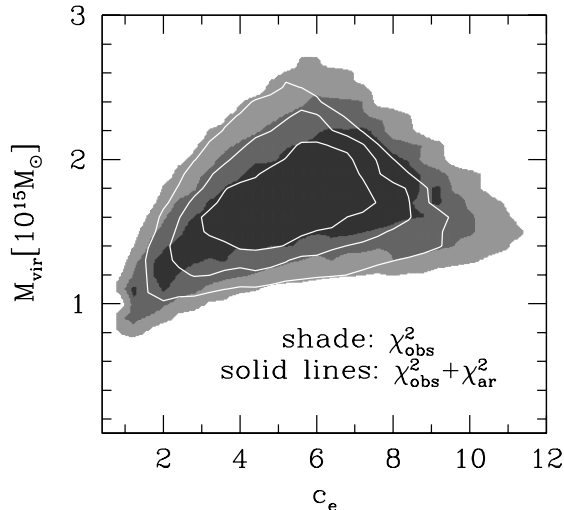


FIG. 4.— As in the previous figure, the constraint contours are shown in the $c_e - M_{\text{vir}}$ plane for the triaxial halo model, where the virial mass M_{vir} is derived from the model parameters constrained in Figure 3. Note that the concentration parameter of the triaxial halo model, c_e , is approximately related to that of the spherical model via $c_e \simeq 0.45c_{\text{vir}}$ (JS02).

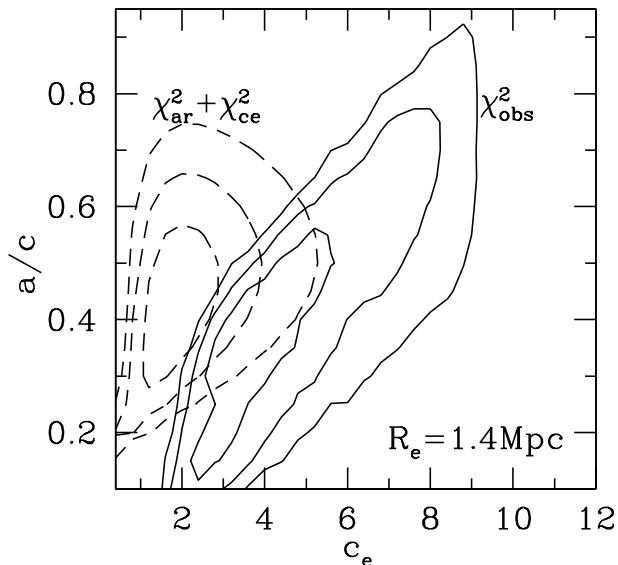


FIG. 5.— Constraint contours (solid lines) in the $c_e - a/c$ plane as in the previous figure, but the radius R_e is fixed to $R_e = 1.4\text{Mpc}$ which is consistent with observational constraints at $1-\sigma$ level (see Table 1). Note that these results include the uncertainties of the other parameters besides R_e . The constraints are directly compared with the theoretical predictions (dashed lines) giving the 68%, 95% and 99.7% probabilities for the c_e and a/c distribution derived using the model of JS02. While the PDF of c_e slightly depends on halo mass, in computing the theoretical predictions we fix the virial mass to $M_{\text{vir}} = 1.5 \times 10^{15} M_{\odot}$ which roughly corresponds to $R_e = 1.4\text{Mpc}$ for a given range of $(c_e, a/c, b/c)$ we have considered here. It is clear that the observation and theory are consistent at $\sim 2-\sigma$ level (see text for more details).

consistent with observational constraints at $1-\sigma$ level. Note that the other parameters are allowed to vary. The clear trend, a smaller c_e is favored with decreasing a/c , is apparent. This result allows a more direct comparison with the theoretical prediction, since JS02 suggested that the halo concentration c_e be tightly correlated with the axis ratio a/c . The PDF of c_e , $p(c_e)$, is given by equation (20) in JS02 (also see Oguri et al. 2003). The PDF is approximated with a log-normal distribution, where the mean value of c_e depends on halo mass, a/c

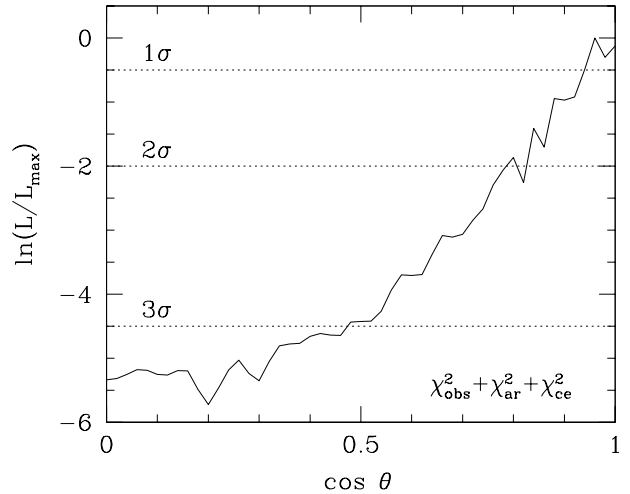


FIG. 6.— The likelihood function against the angle parameter θ between the major axis of triaxial halo and the line-of-sight direction, assuming the priors for the PDFs of axis ratios and halo concentration. The horizontal dotted lines show 68%, 95%, 99.7% confidence limits ($\Delta\chi^2 = 1, 4$ and 9 , respectively). It is clear that an alignment of the halo elongation along the line-of-sight is favored in order for the CDM-based halo model to match the A1689 lensing measurements.

and redshift (see eq. [23] in JS02) and the standard deviation $\sigma(\ln c_e) \approx 0.3$. Combining with the PDFs (eq. [6]) for the axis ratios, the dashed contours in Figure 5 show the 1-, 2- and 3- σ probabilities for the c_e and a/c parameters, expected for a halo at $z = 0.18$, which are estimated from $\chi_{\text{ar}}^2 + \chi_{\text{ce}}^2 = 2.3, 6.17$, and 11.8 , respectively, where $\chi_{\text{ce}}^2 = -2\ln[p(c_e)]$. It is clear that the observation and theory overlap at $\sim 2-\sigma$ level. To see this more quantitatively, we compute the fraction of halos whose axis ratio a/c and concentration parameter c_e fall inside the contours constrained from the observation. We find that, if we take 1-, 2-, and 3- σ limits as the observational constraints, then the fraction becomes 2.7%, 6.1%, and 11.6%, respectively. In contrast, if we *a priori* assume the spherical halo model (B05a), the fraction is significantly reduced to $< 0.1\%$, even if we take the 3- σ limit as observational constraints. Hence, we conclude that the A1689 lensing measurements are indeed compatible with the CDM-based triaxial halo model, if the A1689 represents a rare population ($\approx 6\%$ fraction) of cluster-scale halos (also see the discussion in the next section).

Finally, we look at the constraints on the angle parameter θ between the major axis and the line-of-sight direction. Figure 6 shows the likelihood function against θ , derived from the observational constraints χ_{obs}^2 plus the theoretical PDFs of axis ratios and concentration parameter, $\chi_{\text{ar}}^2 + \chi_{\text{ce}}^2$. One can find $\cos\theta > 0.8$ ($\theta < 37^\circ$) is obtained at $2-\sigma$ level. Thus the major axis of the triaxial halo, when the halo has a reasonable concentration of $c_e = 1 - 2$, is favored to be aligned with the line-of-sight direction in order to match the A1689 steep mass profile.

4. SUMMARY AND DISCUSSION

In this paper, we have employed the triaxial halo model of JS02 to extract more reliable information on the three-dimensional mass distribution of the massive cluster A1689, from the precise lensing measurements done based on the ACS and Subaru data. We have shown several important results. First, based on the simple thought experiment in §2, it was demonstrated that the halo triaxiality could cause a sig-

nificant bias in estimating the virial mass and concentration parameter from the lensing information, if a spherical halo model is *a priori* assumed for the model fitting (see Figure 2). In particular, both the virial mass and concentration parameter are overestimated (underestimated) when the triaxial halo is projected along the major (minor) axis. Second, we derived constraints on the parameters of the triaxial halo model from the fitting to the lensing measurements of A1689, by changing all 7 parameters that specify the triaxial model; the *virial* radius and concentration parameter of the triaxial modeling, two axis ratio parameters, and three angle parameters that determine the halo orientation. We have shown that the halo triaxiality significantly weakens the parameter constraints, compared to those derived when *a priori* assuming the spherical halo model. In addition, the parameter constraints are strongly degenerate, mainly because of a lack of the halo shape information along the line-of-sight (see Table 1 and Figures 3 and 4). As a result, the triaxial halo model with a theoretically expected halo concentration $c_e = 1 - 2$ is acceptable at $1-\sigma$ level, while the halo shape parameters (axis ratios and orientation) are hardly constrained. To further improve the model constraints, we used the theoretical predictions of probability distributions for the halo shapes, derived in JS02, as the priors to the model fitting (see Figures 3, 4, 5 and 6). Most interestingly, we found that about 6% population of cluster-scale halos, expected from the CDM structure formation, can match the A1689 mass profile, if the major axis is almost aligned with the line-of-sight direction. Hence, although it has been shown that the triaxiality has a great impact on strong lensing probabilities (Oguri et al. 2003; Dalal et al. 2004; Oguri & Keeton 2004), our results clearly demonstrate that the halo triaxiality is also very important for exploring the three-dimensional mass distribution of an individual cluster from the lensing measurements.

It is encouraging that the triaxial halo model yields the lensing-constrained mass of A1689 consistent with the mass estimate derived from the *X*-ray observation at $3-\sigma$ level (see Figure 4), while the significant discrepancy of factor 2 has been reported in the literature (Miralda-Escude & Babul 1995; Andersson & Madejski 2004; B05b). We have checked that the consistent mass estimate appears when the major axis of the triaxial halo is oriented along the line-of-sight direction, as inferred from Figure 2. Note that the *X*-ray mass estimate is likely to be less affected by the halo triaxiality than the lensing, as described in Gavazzi (2005). Therefore, it is interesting to notice that the triaxial halo elongated along the line-of-sight could resolve both the previously reported discrepancies of the high concentration as well as of the lensing and *X*-ray mass estimates. Unfortunately, however, this hypothesis cannot be further tested by the lensing information alone we have used, because the halo shape parameters (axis ratios and orientation) could not be well constrained. Improving the halo shape constraints will allow us to make a more

severe, quantitative test of the triaxial halo model, as it is clear from Figure 3. This would be possible by combining the lensing measurements with the detailed observations of kinematics, *X*-ray emission and/or the Sunyaev-Zel'dovich (SZ) effect, since projections affect the observables in different ways (e.g., Girardi et al. 1997; Zaroubi et al. 2001; Marshal et al. 2003).

While our triaxial modeling is much more realistic than the simple spherical fit, there is still room for improvement. A caveat is that the PDFs of axis ratios and concentration (JS02) were derived for less massive clusters ($M_{\text{vir}} \lesssim 10^{14} M_{\odot}$). Thus it is unclear if the extrapolated predictions still hold for very massive clusters ($M_{\text{vir}} \gtrsim 10^{15} M_{\odot}$) considered here. More importantly, the selection effect, which we have neglected in this paper, might be important. A1689 is well known as the strong-lensing cluster, with the largest Einstein radius ($\sim 50''$). Strong lensing probabilities are very sensitive to shapes and orientations of dark halos such that a halo with large triaxiality, high concentration and the major axis aligned with line-of-sight has higher lensing probabilities (Oguri et al. 2003; Dalal et al. 2004; Oguri & Keeton 2004). Therefore A1689 might be indeed such a cluster, as implied in this paper. Thus taking into account the selection effect could further reduce the discrepancy of A1689 (e.g., Hennawi et al., in preparation). However, in practice it is quite difficult to quantify the selection effect. For strong lens systems discovered in a well-defined homogeneous survey, such as the large-separation lensed quasar SDSS J1004+4112 (Inada et al. 2003; Oguri et al. 2004), it will be possible to take this selection effect into account in a correct manner.

Another important implication we have found is that the halo triaxiality can be a source of systematic errors in estimating the virial mass from the lensing measurement. While it has been shown that the lensing-based mass determination suffers from the projection effect due to an intervening matter, not necessarily associated with a cluster of interest (Metzler et al. 2001; Wambsganss et al. 2005), our results imply that the halo shape itself causes a bias in the mass determination (also see Bartelmann 1995; Clowe et al. 2004; Hamana et al. 2004). The accurate mass determination is crucial to achieve the full potential of future cluster cosmology experiments such as expected from Planck, where the cluster redshift distribution is measured to constrain cosmological models (Haiman et al. 2001). Therefore, it is again very interesting to address how the mass determination can be improved for an individual cluster as well as in a statistical sense by combining the lensing, *X*-ray and SZ effect measurements.

We thank Jounghun Lee for useful discussion. M.O. is supported by JSPS through JSPS Research Fellowship for Young Scientists.

REFERENCES

- Andersson, K. E., & Madejski, G. M. 2004, *ApJ*, 607, 190
 Bartelmann, M. 1995, *A&A*, 299, 11
 Broadhurst, T., Takada, M., Umetsu, K., et al. *ApJ*, 619, L143 (B05a)
 Broadhurst, T., et al. *ApJ*, 621, 53 (B05b)
 Bullock, J. S., Kolatt, T. S., Sigad, Y., Somerville, R. S., Kravtsov, A. V., Klypin, A. A., Primack, J. R., & Dekel, A. 2001, *MNRAS*, 321, 559
 Clowe, D., De Lucia, G., & King, L. 2004, *MNRAS*, 350, 1038
 Dalal, N., Holder, G., & Hennawi, J. F. 2004, *ApJ*, 609, 50
 Gavazzi, R. 2005, *A&A*, submitted (astro-ph/0503696)
 Gavazzi, R., Fort, B., Mellier, Y., Pello, R., & Dantel-Fort, M. 2003, *A&A*, 403, 11
 Girardi, M., Fadda, D., Escalera, E., Giuricin, G., Mardirossian, F., & Mezzetti, M. 1997, *ApJ*, 490, 56
 Haiman, Z., Mohr, J., & Holder, G. 2001, *ApJ*, 553, 322
 Hamana, T., Takada, M., & Yoshida, N. 2004, *MNRAS*, 350, 893
 Inada, N., et al. 2003, *Nature*, 426, 810
 Jing, Y. P., & Suto, Y. 2002, *ApJ*, 574, 538 (JS02)
 Kneib, J., et al. 2003, *ApJ*, 598, 804
 Lee, J., Jing, Y. P., & Suto, Y. 2005, *ApJ*, submitted (astro-ph/0504623)

- Marshall, P. J., Hobson, M. P., & Slosar, A. 2003, MNRAS, 346, 489
- Metzler, C. A., White, M., & Loken, C. 2001, ApJ, 547, 560
- Miralda-Escude, J., & Babul, A. 1995, ApJ, 449, 18
- Navarro, J. F., Frenk, C. S., & White, S. D. M. 1997, ApJ, 490, 493
- Oguri, M., Lee, J., & Suto, Y. 2003, ApJ, 599, 7
- Oguri, M., et al. 2004, ApJ, 605, 78
- Oguri, M., & Keeton, C. R. 2004, ApJ, 610, 663
- Schneider, P., Ehlers, J., & Falco, E. E. 1992, Gravitational Lenses (Heidelberg: Springer)
- Schneider, P., King, L., & Erben, T. 2000, A&A, 353, 41
- Wambsganss, J., Bode, P., & Ostriker, J. P. 2005, ApJ, submitted (astro-ph/0405147)
- Zaroubi, S., Squires, G., de Gasperis, G., Evrard, A. E., Hoffman, Y., & Silk, J. 2001, ApJ, 561, 600